Martín A. Toderi, Bibiana D. Riquelme, and Gustavo E. Galizzi "Biospeckle laser as a tool to analyze erythrocyte aggregation," Optical Engineering 61(12), 124101 (2 December 2022). https://doi.org/10.1117/1.OE.61.12.124101

Biospeckle laser as a tool to analyze erythrocyte aggregation

Martín A. Toderi,[a,b,*] **Bibiana D. Riquelme**,[b,c] and **Gustavo E. Galizzi**[b,d]

[a]University of California, Los Angeles, Department of Physics and Astronomy, Los Angeles, California, United States
[b]Instituto de Física Rosario (CONICET-UNR), Rosario, Argentina
[c]UNR, Facultad de Cs. Bioquímicas y Farmacéuticas, Rosario, Argentina
[d]UNR, Facultad de Cs. Exactas, Ingeniería y Agrimensura, Rosario, Argentina

Abstract. We analyze the erythrocyte aggregation by the biospeckle laser phenomenon and calculate characteristic parameters to develop non-invasive hemorheological techniques. Biospeckle is more complex than other light-based techniques, such as light transmission, providing information about the dynamics of the scatterers, their size, and morphology. Dextran 500 kDa combined with plasma and phosphate-buffered saline was used to induce controlled *in vitro* erythrocyte aggregation. Red blood cell aggregation was studied using an objective speckle setup in a microchip sample chamber. The speckle grain sizes were determined, and parameters to characterize the morphology of the erythrocyte aggregates were proposed. The inertia moment and the correlation coefficient were determined to assess the cells aggregation dynamics. [DOI: 10.1117/1.OE.61.XX.XXXXXX]

Keywords: biospeckle; red blood cell aggregation; correlation coefficient; inertia moment; microcirculation.

Paper 20220709G received Jun. 28, 2022; accepted for publication Nov. 16, 2022.

1 Introduction

The erythrocyte aggregation phenomenon has been of interest for many years. Most studies involve various scientific areas, such as blood rheology (or hemorheology), biomechanics, clinical medicine, and *in vivo* observations.

During blood circulation, the erythrocytes or red blood cells (RBCs) interact with other blood cells and with those of the vessels. These interactions are usually mediated by adhesion molecules, being of particular interest the erythrocyte–erythrocyte interactions.[1] Normally, human RBCs form aggregates of face-to-face linear structures, resembling a stack of coins called *rouleaux*.[2,3] Following this behavior, *rouleaux* suspended in plasma contain a variable cell number, and they aggregate in branched three-dimensional (3D) structures.

The study of the role of plasma proteins and macromolecules in RBC aggregation continues to be of interest. The linking of fibrinogen to the RBC has been experimentally demonstrated.[4] Other studies have been conducted on the effects of macromolecules in such systems.[5,6] The polysaccharide dextran of 500 kDa of molecular weight (dex500) is frequently used as an RBC aggregation promoter for *in vitro* experimentation.[7] There are two coexisting models to explain the origin of the RBC aggregation. On the one hand, the "bridging" model considers the absorption of macromolecules on the erythrocyte membrane and therefore a possible adhesion between two cells as the origin of the *rouleaux*.[8,9] On the other hand, the theory of "depletion" involves a colloidal osmotic pressure caused by macromolecules as the main reason for the *rouleaux* formation.[10,11] These models have been experimentally tested and discussed, giving a new combined theory derived from colloid physics.[12]

*Address all correspondence to Martín A. Toderi, mtoderi@physics.ucla.edu

0091-3286/2022/$28.00

Research based on computational simulation relied on experimental results and has explored the individual RBC rheology,[13,14] and its collective behavior under different types of flow.[15] In vascular diseases (diabetes and hypertension), the shape of the RBC aggregates is altered, which may lead to obstructions in blood microcirculation. The lower content of sialic acid disturbs the rheological properties of the membrane, and more adhesion disorderly occurs. Moreover, it has been observed that in pathologies with deficiency of membrane sialic acid, the erythrocyte adhesion force is greater, and large spheroidal aggregates called "clusters" appear.[16,17]

Micrometric-scale circulation is of interest, since hemodynamic difficulties related to pathologies frequently occur due to the formation of clusters of RBCs, which difficult passage through the blood microvessels.[18,19] More general studies made it possible to extend the field of research and apply the effects of erythrocyte adhesion to the analysis of more complex processes, such as coagulation,[20] and to delve into more specific aspects of biology, such as the agglutination by antibodies that interact with the erythrocyte.[21–23]

Blood vessel obstructions reduce disaggregation forces increasing RBC aggregate sizes, which amplify the flowing difficulty, causing a feedback situation.[24] The erythrocyte aggregation characterization through sensitive parameters is a valuable aid to analyze possible alterations in the microcirculation observed in vascular pathologies.[16,25,26]

In this work, we investigate the application of the biospeckle laser (BSL) technique to characterize the aggregation of RBCs as light-based technologies have great potential to develop non-invasive tools for human healthcare.

2 BSL Theory

It is usual to study the kinetics of erythrocyte aggregation by light transmission,[27] but the BSL technique could provide more information about the phenomenon, having a more complex approach. This method records the variation of scattered light intensity in two dimensions through time, obtaining sequences of "images" to extract information of the physical phenomenon.

The speckle effect occurs when an optically rough surface is illuminated by coherent light. At a distant point of observation, an optical field is obtained from the light scattered by each illuminated surface point. Due to the random nature of the distribution of scattering elements on the surface, the initial values of the complex field of these elementary waves will also take random values. Therefore, the value of the optical field will vary randomly for different observation points.[28] In this way, a spatial distribution of light and dark points is obtained as a consequence of constructive or destructive interference (see Fig. 1).

Speckle laser-based techniques have recently been transferred to the field of biomedicine from the area of optical metrology. In particular, the *biospeckle* is the product of a speckle pattern that varies over time due to an ongoing biological process. Several recent works have explored the BSL technique to characterize the dynamics of biological systems, determination of functional vascular density, chemotaxis, and motility of microorganisms, detection of fungi, and the study of microvascular blood circulation.[29–32] The biological process of interest in this work is the RBC aggregation. In particular, the characterization of the *rouleaux* formation process under 2
different RBC aggregation conditions. Previously, we worked with subjective BSL and found indexes of interest for characterizing the erythrocyte dynamics and parameters indicators of the ratio of the volume of RBCs to the total volume of blood known as hematocrit.[33]

The size of the speckle grain observed in the light scattered by an optically rough surface depends on the illuminated area and the position of the observation plane, but not on the optical system used to visualize it. For this reason, this type of speckle is referred to as *objective speckle*. Consequently, as stated by Jones and Wykes,[28] the mean speckle grain size reduced to one dimension d_{sp} is

$$d_{sp} = \frac{\lambda z}{l_0}, \tag{1}$$

where the illuminated area is considered to have dimensions $l_0 \times l_0$, λ is the wavelength of the incident light, and z is the distance to the scattering surface. This work is focused on

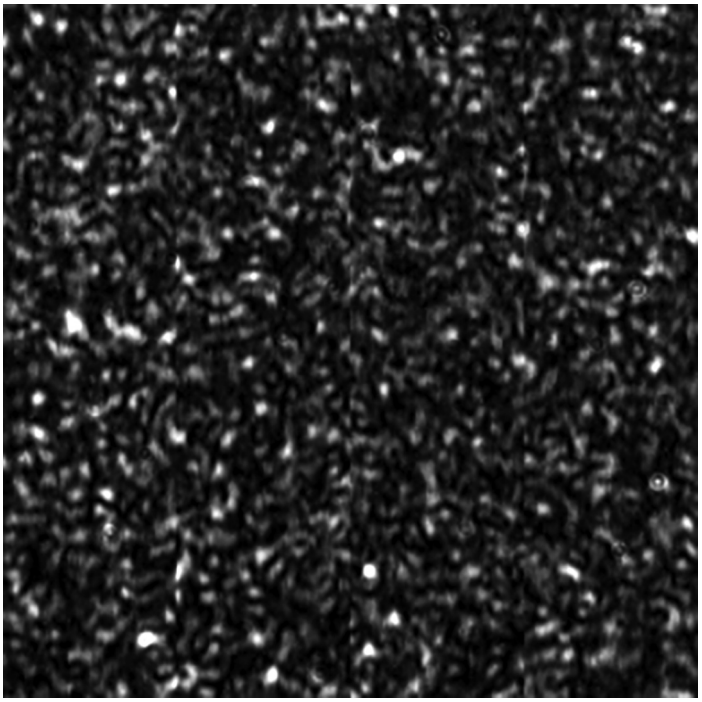

Fig. 1 Speckle distribution obtained from a fresh blood sample.

an objective biospeckle setup, allowing the recording of changes in the grain size of the BSL pattern.

3 Materials and Methods

3.1 *Sample Preparation*

Peripheral blood samples from five healthy donors were used. Blood was drawn by venipuncture and anticoagulated with EDTA. RBCs were obtained from whole blood by centrifugation at 1500g for 5 min at 24°C. The plasma phase was separated, buffy-coat was discarded, and the RBCs were washed three times with saline, following the international recommendations for hemorheological studies.[34] In parallel, the morphological integrity of the cells was verified by microscopy.

Suspensions of RBC in different media with dex500 were prepared to evaluate the characteristic parameters of the BSL technique. RBC suspensions were obtained by mixing plasma or a solution of phosphate-buffered saline (PBS) with dex500 solutions. For the latter, preparation of the suspension media was carried out by replacing autologous plasma with PBS, EDTA (0.056%), and albumin (Sigma, A9511-10G Lot# 107K7560V) at 0.5%. Albumin is necessary to prevent the glass effect on RBCs and to maintain the integrity of the cells. Dex500 (500 kDa molecular weight) was added to induce the formation of erythrocyte aggregates.[7] To achieve this, a 10% dex500 stock solution in PBS was prepared and mixed with the suspension medium to obtain 0.2, 0.4, 0.6, 0.8, and 1.2 g/dL dex500 solutions. Hematocrit was fixed to 40%, similarly to the average physiological range.

3.2 *Experimental Setup*

The sample chamber was a previously developed optical chip with a circular test cavity of 15 μL of volume, as described by Toderi et al.[27] The objective BSL experimental setup, schematized in Fig. 2, employed a He-Ne laser ($\lambda = 632.8$ nm, 60 mW, Melles Griot) to illuminate the blood sample. A dimmer was used to adjust the intensity of the laser beam, the area of illumination was controlled by a 10× expansion lens (EL), and a pinhole was utilized to obtain uniform

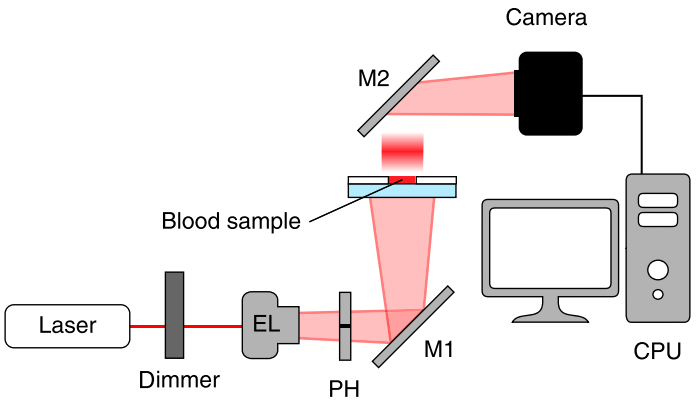

Fig. 2 Schematic representation of the objective BSL experimental setup, side view. EL, expansion lens; PH, pinhole; M, mirror.

illumination of the sample. The optical chip was placed in the beam path between two mirrors, M1 and M2. Mirror M2 allowed the observation of the forward scattered light, obtaining an image of forward scattering BSL (FSC-BSL). Data were recorded by a video camera (Dalsa model CA-D6, 256×256 pixels, 10×10 μm pixel) externally controlled by a frame grabber (Coreco Imaging PC-DIG) and a CPU. The experiments were performed at controlled room temperature of 24°C, and the system was mounted on an optical table (Melles Griot) to avoid interference from external mechanical vibrations. It is worth mentioning that the average light intensity increases throughout the experiment as the aggregation process occurs. Consequently, the light intensity was adjusted to obtain the best BSL image quality for each experiment. In this way, the average intensity is not determined by the specific characteristics of each sample, and its variation in time would not affect the data processing.

3.3 *Data Acquisition and Analysis*

The blood sample was gently mixed several times and then injected into the optical chip. Immediately after, the chip was positioned, and the sample was left unperturbed. At a sampling rate of 8 frames per second (fps), 2000 images were registered during 250 s. The BSL distributions were processed by custom software, creating a 3D matrix composed by the intensity map of the pixels for each frame along time. To improve the identification of the information corresponding to the dynamic behavior of the RBCs, a software-implemented quadrature mirror filter based on the discrete wavelet transform was applied to the recorded data.[35,36] In previous work, we proposed that the lower coefficients of this decomposition allowed us to better isolate the signal from mechanical fluctuations of the suspension medium.[33]

3.3.1 *Biospeckle parameters*

Through computational algorithms, it is possible to acquire information on the kinetics of RBC aggregation, aggregate morphology, and other characteristics of interest from the analysis of BSL distributions. For this purpose, the following parameters based on numerical calculation were obtained.

The correlation coefficient (CC) between the first image and the following ones is defined as[33]

$$\mathrm{CC}(k) = \frac{\left\langle I(0)I(k)\right\rangle - \left\langle I(0)\right\rangle\left\langle I(k)\right\rangle}{[(\langle I^2(0)\rangle - \langle I(0)\rangle^2)(\langle I^2(k)\rangle - \langle I(k)\rangle^2)]^{1/2}}, \tag{2}$$

where k is the frame number that assumes values from $0, 1, \ldots, (K-1)$ with K the total number of images from the sequence recorded during the experiment; $I(k)$ is a two-dimensional matrix composed by the gray levels of each pixel corresponding to frame k; and $\langle\rangle$ denotes the mean

value operator. The operations between matrices, such as product and square, are performed on an element-to-element basis. The operator $\langle\rangle$ is the arithmetic mean of the matrix elements. This coefficient provides a quantitative comparison of the similarity of each biospeckle pattern $I(k)$ of the sequence of images with respect to the first one $I(0)$ chosen as the reference state.

The inertia moment (IM) is defined as[33,37]

$$\mathrm{IM} = \sum_i \sum_j \frac{\mathrm{COM}(i,j)}{\mathrm{Norm}} |i-j|^2, \tag{3}$$

where i and j are the matrix coordinates, Norm is the normalization of the co-occurrence matrix (COM),[38] and COM is calculated from the time history speckle pattern (THSP).[39] The THSP was constructed from a random Gaussian distribution selection of points around the central pixel of the first frame for each calculation. The COM evaluates the dispersion of consecutive pixel values in the THSP, representing a transition histogram of intensity. The higher the activity is, the wider the spreading around the main diagonal results is.[33] Then, the spreading around the main diagonal can be quantified by the IM.

When evaluating the CC, fast loss of correlation was observed for the high-frequency band regardless of the RBC sample and the initial time considered for the CC. By contrast, the CC showed variations in time for the low-frequency band, implying different decorrelation evolution. These results suggest that data from the low-frequency bandwidth are related to the aggregation conditions, which are the experiments' changing factors. The high-frequency bandwidth would mainly contain information about the suspension medium fluctuations, where the mechanical characteristics of the fluid remain unchanged. Similar observations were reported by Braga et al.[40,41] for plants, seeds, and sperm. These medium fluctuations would not be attributed to external mechanical vibrations, but to local internal turbulence inherent to the system. Regarding the IM, the discrimination of the signal only globally shifted the values and did not change the trends observed over different sample conditions. Consequently, we used the full signal for IM calculations.

The normalized autocovariance function was calculated for each frame from the intensity distribution recorded in the 3D matrix to study the time evolution of the grain size of the BSL pattern. This method uses the intensity autocorrelation function that measures the average radius of a speckle grain.[42] Considering the autocorrelation function for the frame $I(x,y)$, as $R_I(x,y)$, where x and y are the spatial coordinates, the normalized autocovariance function of the intensity $\mathrm{AC}_I(x,y)$ is

$$\mathrm{AC}_I(x,y) = \frac{R_I(x,y) - \langle I(x,y)\rangle^2}{\langle I(x,y)^2\rangle - \left\langle I(x,y)\right\rangle^2}. \tag{4}$$

$R_I(x,y)$ is obtained from applying the inverse Fourier transform (FT^{-1}) to the power spectral density (PSD) of the intensity written as

$$\mathrm{PSD}_I(v_x, v_y) = |\mathrm{FT}[I(x,y)]|^2, \tag{5}$$

where FT is the Fourier transform.

Therefore, combining Eqs. (4) and (5), the normalized autocovariance function of the intensity results

$$\mathrm{AC}_I(x,y) = \frac{\mathrm{FT}^{-1}[|\mathrm{FT}[I(x,y)]|^2] - \langle I(x,y)\rangle^2}{\langle I(x,y)^2\rangle - \langle I(x,y)\rangle^2}. \tag{6}$$

Then, the full width at half maximum (FWHM) of the function AC_I is defined as a_h and a_v for the horizontal profile $\mathrm{AC}_I(x,0)$ and the vertical profile $\mathrm{AC}_I(0,y)$ as depicted in Fig. 3.

These parameters provide information representative of the dimensions of the BSL grain. Moreover, $S_g = a_h \times a_v$ was defined as an approximation of the area occupied by the BSL grain.

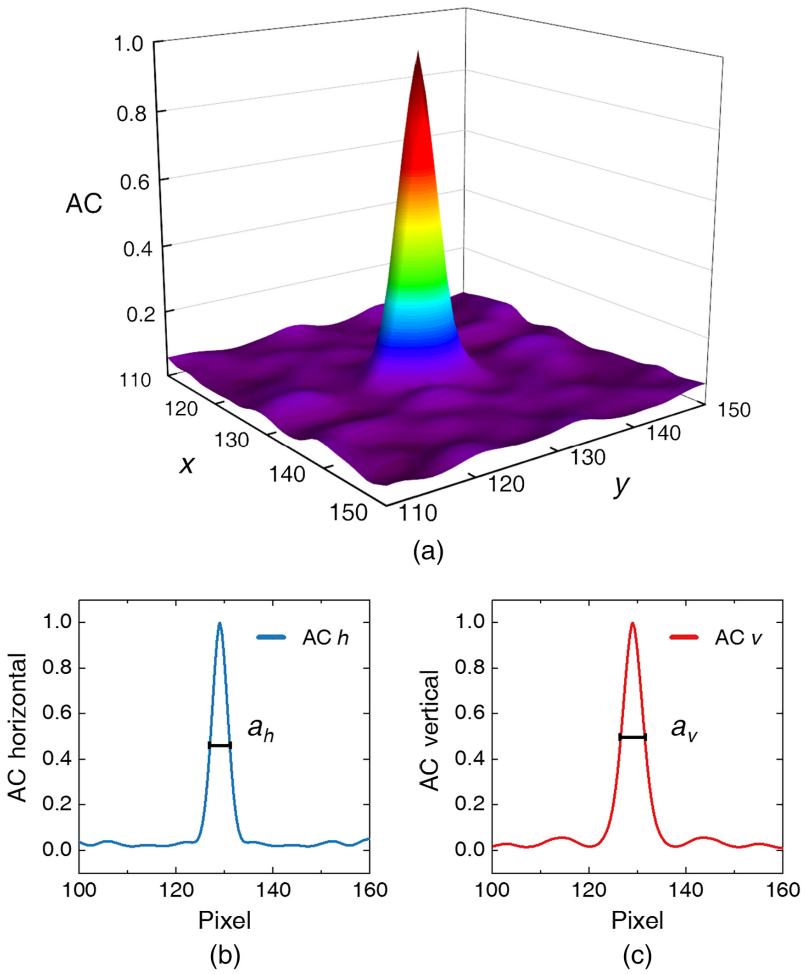

Fig. 3 3D reconstruction of the autocovariance function for a particular frame of the BSL collection obtained from (a) blood sample, (b) horizontal profile and FWHM, a_h, and (c) vertical profile and FWHM, a_v.

In our experiments, the calculation of each BSL parameter includes a normalization process so that the variation of the average intensity over time does not significantly affect the final result.

In addition, parallel determinations were performed with a previously developed optical chip aggregometer based on light transmission.[27] This device registers the intensity of light transmitted through a blood sample, which changes in time due to the aggregation process, giving curves called syllectograms. The same test chamber geometry and sample management make it possible to compare the two methods.

4 Results

As previously introduced, it is known that dex500 alters the adhesion mechanism of the erythrocytes, and depending on its concentration in the suspension medium, different degrees of RBC aggregation occur.[7] As the blood sample shows activity over time due to RBCs dynamics, the "illuminated area" varies according to the formation of structures by cell adhesion. In the case of increased erythrocyte aggregation resulting in large *rouleaux* or *clusters*, a decrease in the illuminated area is expected due to the smaller number of isolated cells.

The studied case is composed of a discontinuous group of scatterers that dynamically change. In this way, the area that produces the scattering phenomenon (the *illuminated area*) is different from the area that the incident beam occupies, which is defined as the *area of illumination*. This

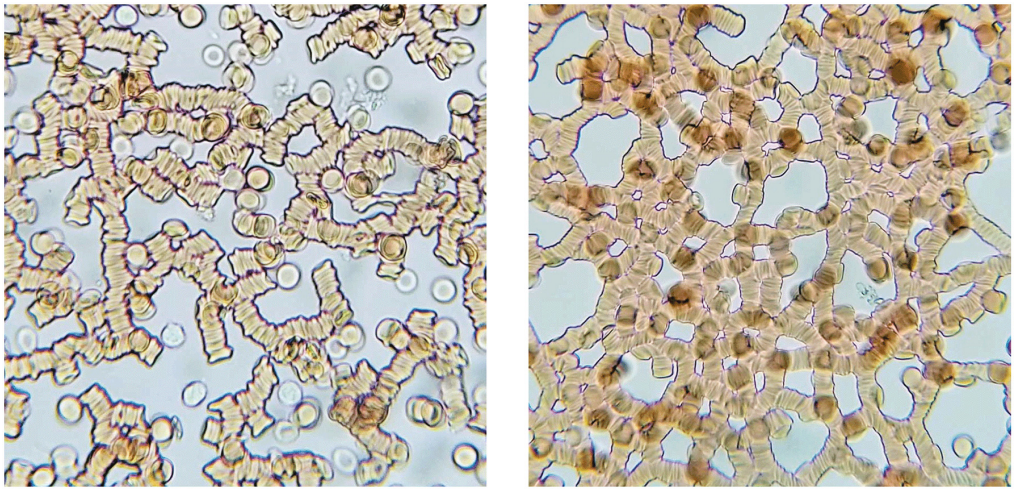

(a) (b)

Fig. 4 RBC aggregates suspended in plasma (a) and plasma with dex500 at 0.8 g/dL (b). RBCs aggregate in branched 3D structures reshaping the scatterers' morphology and overall characteristics of the illuminated surface, changing how light gets transmitted and scattered. Images from the optical microscope with 40× objective lens, hematocrit 2.5%.

terminology refers to the idea that the change in the scattering area influences the grain size of the speckle. The denominator in Eq. (1) is the area conformed by the scatterers that, in this case, is not the same as the area that the beam occupies. Recalling Eq. (1), reducing the illuminated area ($l_0 \times l_0$) increases the BSL grain size. Figure 4 shows visual confirmation of the aggregates for a hematocrit suitable for microscopic observation. All other microscopic images of RBC aggregation that follow the same consideration as a physiological range hematocrit are not suitable for imaging. Aggregates formation occurs in the same way for higher hematocrits, such as 40%, which was used in all experiments.

The BSL grain size presented variations according to different dex500 concentrations in the sample, reinforcing the hypothesis of the feasibility of using the objective BSL as a descriptor of the erythrocyte aggregation phenomenon. In addition, the behavior of the CC and IM parameters showed sensibility to these RBC aggregation alterations. Sections 4.1 and 4.2 present the results for RBC suspended in autologous plasma and in PBS, both mixed with several concentrations of dex500.

4.1 *RBCs Suspended in Plasma with dex500*

In these experiments, RBCs are in contact with proteins, electrolytes, and other plasma elements. The fibrinogen is one of those plasmatic proteins favoring the binding of the cells and consequently promoting the formation of *rouleaux*. Dex500 is added to this medium, so the aggregation studied is due to the superposition of the two factors. The BSL parameters previously described were evaluated, and the following results were obtained.

The CC presented different variations according to the concentration of dex500 present in the sample (see Fig. 5). The decay of the CC is less pronounced as the erythrocyte aggregation increases due to the effect of the polysaccharide in the formation of the bonds between RBCs [see Figs. 5(a)–5(c)]. Curves are shown for different initial reference times, 60, 120, and 180 s. Considering the evolution of CC as an exponential function, the dependency of CC was linearized by applying the natural logarithm. From the linear fitting slope, the correlation index (CI) was obtained. In this way, a single value of CI is obtained for each sample and every CC initial reference time. Figure 5(d) shows that the CI presents minimal variations with the reference time in media with dex500. In contrast, the control sample has a noticeable increment of the CI. Overall, the CI exhibits higher values when dex500 is present in the media.

Recently, Toderi et al.[33] proposed that IM varies with hematocrit, using a BSL subjective experimental setup. Here, Fig. 6(a) shows that IM remains constant within the uncertainty for

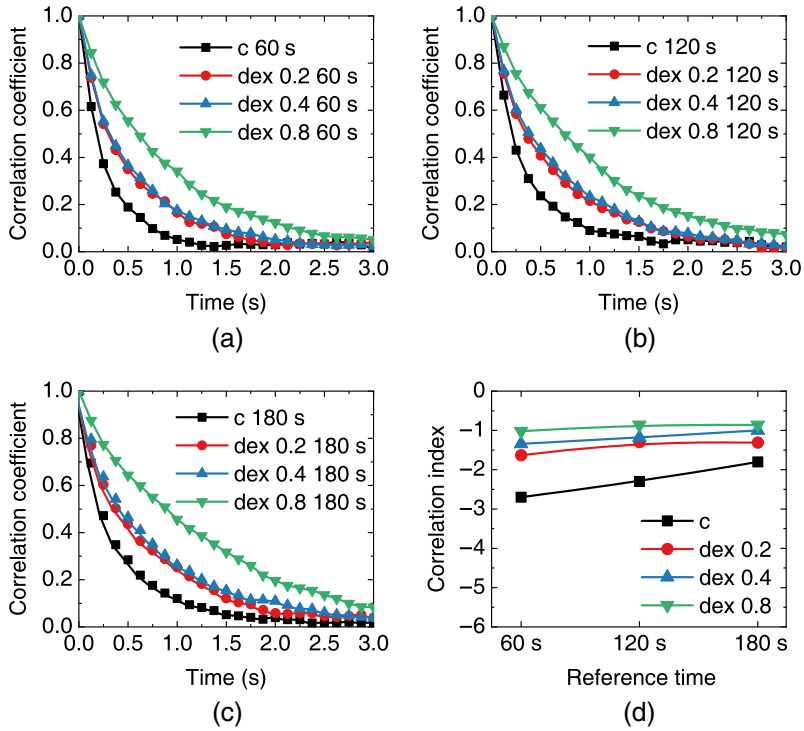

Fig. 5 CC for RBCs suspended in plasma with dex500 at 0.2, 0.4, and 0.8 g/dL for different initial reference times: (a) 60 s, (b) 120 s, and (c) 180 s, respectively. CI for RBCs suspended in plasma with dex500 at 0.2, 0.4, and 0.8 g/dL, c is the control without dex500. (d) Horizontal axis represents the initial reference time at with the respective CC is calculated.

different dex500 concentrations, supporting the previous hypothesis. Thus, we propose that IM would not depend on the bonds favored by molecules that activate aggregation but on the RBC concentration for the case of presence of plasma proteins. Figure 6(b) presents transmitted light intensity as a function of time (syllectogram) registered with the optical chip aggregometer. Curves of faster growth and greater amplitude are observed for increasing dex500 concentrations.

Variations in the BSL grain size were observed over time and between different samples. Figure 7(a) depicts the grain size for each dex500 concentration. Also, the figure shows the percentage variation obtained from the beginning to the end of the measurement ($\Delta\%$). Experimental data were fitted with a cubic polynomial: $\mathrm{Int0} + \mathrm{B1}x + \mathrm{B2}x^2 + \mathrm{B3}x^3$, giving three

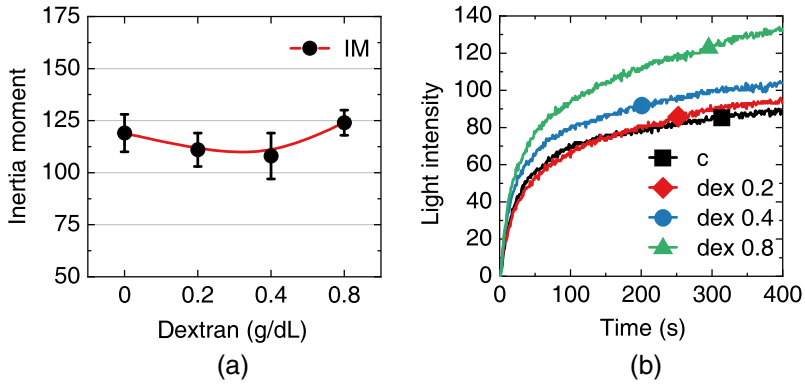

Fig. 6 (a) BSL parameter IM as a function of dex500 concentration in plasma, the error bars represent the standard deviation. (b) Syllectograms registered with the optical chip aggregometer for RBCs suspended in plasma with dex500 at 0.2, 0.4, and 0.8 g/dL.

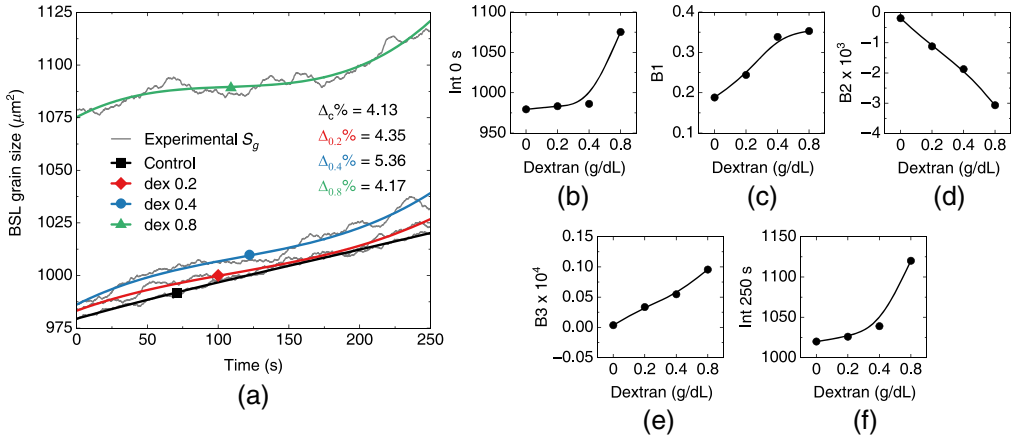

Fig. 7 (a) Time evolution of the BSL grain size for RBCs in plasma with dex500, fitted by a polynomial: $\mathrm{Int0} + \mathrm{B1}x + \mathrm{B2}x^2 + \mathrm{B3}x^3$. Variation of polynomial fitting coefficients with dex500 concentration: (b) Int0, (c) B1, (d) B2, and (e) B3. (f) The value of the grain size at the end of the measurement.

adjustment coefficients. In addition, the intersections of the polynomials with the vertical axes corresponding to 0 and 250 s were defined as parameters. Figures 7(b)–7(f) show the variation of these parameters for the dex500 concentration. Monotonous behaviors are observed, mostly with increasing tendencies as more dex500 is present in the sample except for B2 that decreased.

A gap in the initial value of the grain size is observed for the 0.8 g/dL dex500 concentration. However, the grain size time evolution is similar to the case of the other dex500 concentrations, but with a more pronounced growth after 200 s. This result could be attributed to the presence of clusters that were not initially disaggregated due to the combined aggregating effect fibrinogen and dex500 at 0.8 g/dL.

4.2 *RBCs Suspended in PBS with dex500*

Similarly to Neu et al.,[7] the suspension of RBCs in PBS with dex500 solution allowed to control the erythrocyte aggregation process. Therefore, only isolated cells were present in the suspension medium without dex500 [see Fig. 8(a)]. As dex500 concentration increases, more complex aggregates were obtained, and large branched *rouleaux* were observed [see Figs. 8(c)–8(f)].

The calculated CC showed slower decorrelation for higher concentrations of dex500. Figure 9(a) shows an example of the CC corresponding to the samples for the initial reference time of 120 s. The presence of more complex structures changes the dynamics of the scatterers, and CC decorrelates more slowly. The linearization of this exponential decay using the natural logarithm and further calculation of the corresponding slope allow us to obtain a single characteristic value (CI), related to the sample behavior. The CI was calculated for each dex500 concentration and every initial reference time (0, 60, 120, and 180 s), as shown in Fig. 9(b). The absolute value of CI diminishes for each initial reference time, indicating a less steep decorrelation. The CI variations decrease at a longer initial reference time because the aggregation process eventually reaches a plateau in activity. Moreover, the final values of CI are different for each dex500 concentration which may be related to the final morphology of the aggregates.

Figure 10(a) shows a decrease of the IM as dex500 concentration increases in PBS. In this way, this index would indicate the lowest accumulated activity of the intensity of the pixels during the recording for 1.2 g/dL of dex500. Moreover, all values were higher than those obtained from RBCs suspended in plasma with dex500. The syllectogram for RBCs in PBS indicates that the transmitted light intensity remains approximately constant as expected. Samples in PBS with dex500 give syllectograms with higher amplitudes of transmitted light and faster initial growths, as shown in Fig. 10(b).

The calculations for the BSL grain size S_g showed more differentiated behaviors than for the samples with plasma. Figure 11(a) depicts S_g for each RBC sample and the corresponding fitted

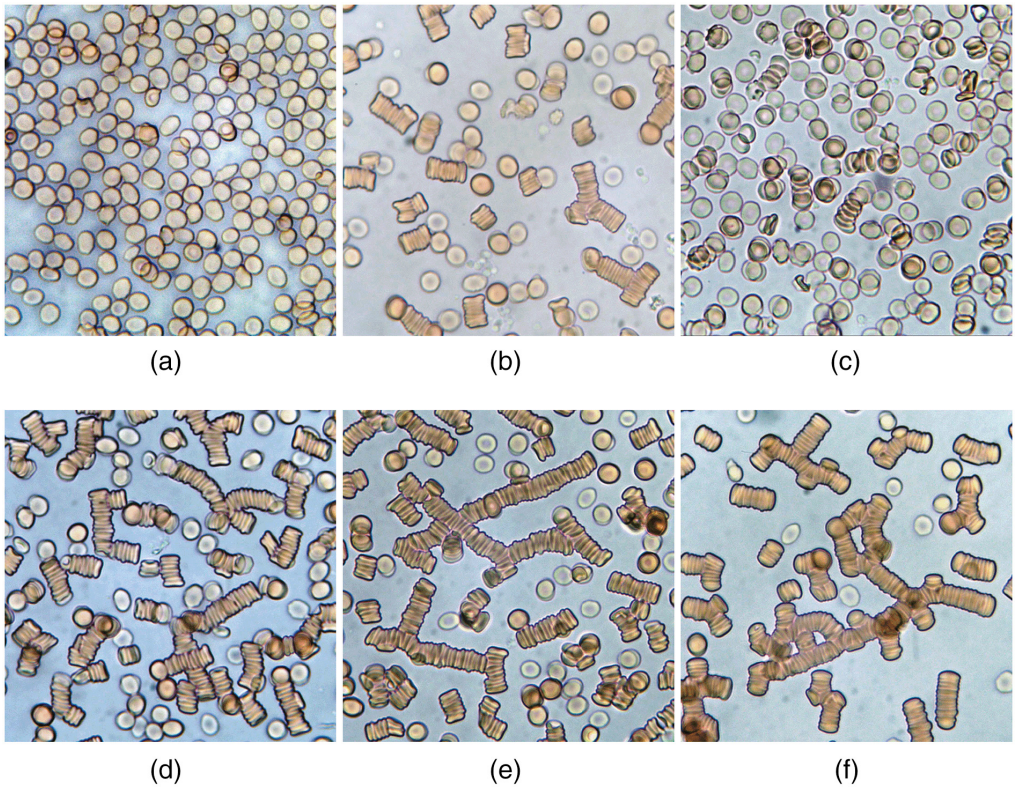

Fig. 8 Visual confirmation of RBC aggregation, a low hematocrit was used to allow observation. RBCs suspended in: (a) PBS, (b) plasma, PBS with dex500 at (c) 0.2 g/dL, (d) 0.4 g/dL, (e) 0.6 g/dL, and (f) 1.2 g/dL. Microscopy images with 40× objective lens, hematocrit 1.5%.

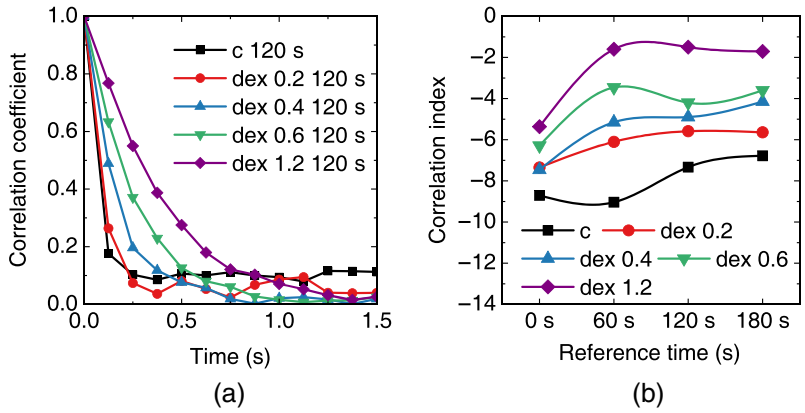

Fig. 9 Results for (a) CC at reference time 120 s and (b) CI as a function of reference time, obtained from RBCs suspended in PBS with dex500 at 0.2, 0.4, 0.6, and 1.2 g/dL; c is the control corresponding to PBS without dex500. Horizontal axis represents the initial reference time at with the respective CC is calculated.

curves. Also, Fig. 11(a) shows $\Delta\%$ values whose amplitude is higher than the obtained for RBCs suspended in plasma. A marked upward trend is observed in the variation of S_g as erythrocyte aggregation increases due to the presence of dex500. Analogously to the case of RBCs in plasma, the experimental data were adjusted through a cubic relationship giving three coefficients (B1, B2, and B3). In addition to the intersections of the polynomials with the axes corresponding to 0 and 250 s, Figs. 11(b)–11(f) show how these coefficients evolve according to the analyzed sample. Throughout the recordings, the coefficients had monotonous behaviors with

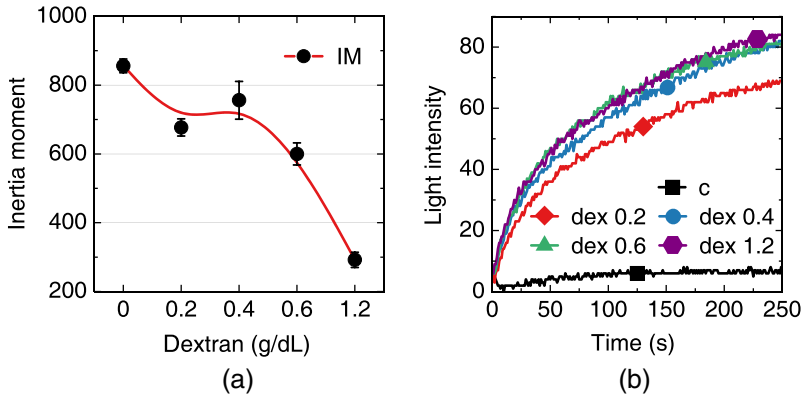

Fig. 10 (a) BSL parameter IM as a function of dex500 concentration in PBS, the error bars represent the standard deviation. (b) Syllectograms registered with the optical chip aggregometer for RBCs samples in PBS with dex500 at 0.2, 0.4, 0.6, and 1.2 g/dL.

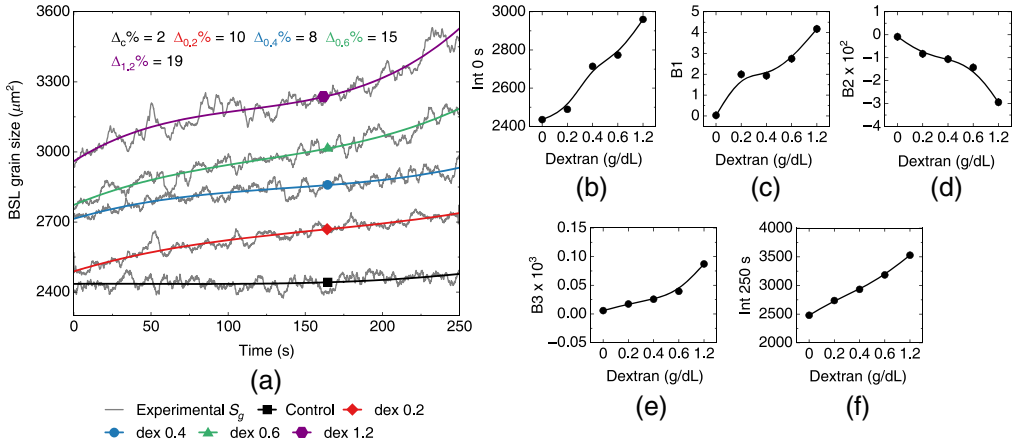

Fig. 11 (a) Time evolution of the BSL grain size for samples with PBS and dex500, fitted by a polynomial of the third degree: Int0 + B1x + B2x^2 + B3x^3. Variation with dex500 concentration of polynomial fitting coefficients: (b) Int0, (c) B1, (d) B2, and (e) B3. (f) The value of the grain size at the end of the measurement.

growing tendencies as dex500 concentration increased, except for the B2 that decreased. Spread values between 2400 and 3000 μm^2 were observed in the initial S_g, which is depicted by Int0 increasing with the concentration of dex500.

5 Discussion

The experiments designed to study the erythrocyte aggregation were performed under a BSL objective configuration with EL to maximize and homogenize the area of illumination. The observations during the BSL experiments allow us to propose the differentiation of the concept of *area of illumination*, i.e., the area occupied by the incident beam in the sample and the *illuminated area*. The illuminated area is the effective surface on which the light encounters an obstacle and is deflected or absorbed, giving rise to the BSL pattern. From the basis of the objective speckle, the grain size of BSL is inversely proportional to the illuminated area if the other variables of the experiment remain constant.

It is important to note that Eq. (1) was used only to introduce the concept of objective speckle formation and the speckle grain size to the experimental case studied. In this case, the speckle grain size was evaluated using the autocovariance function. Other authors studied the grain size

variations in objective speckle. For example, Piederriere et al.[43] observed variations in speckle size related to the change of scatterers' morphology while maintaining the invariance of the area of illumination. In our experiments, the RBCs are the only factor that introduces variables since the beam expansion is fixed throughout the entire measurement. Thus, the variations in grain size are associated with variations of the illuminated area attributed to changes in the 3D morphology and distribution of the scattering elements. Given this, it is possible to formulate indirect monitoring of the formation of different structures, such as *rouleaux* or *clusters*. The syllectograms [Figs. 6(b) and 10(b)] show an increase of the light intensity over time as there is less interaction with larger and more spaced apart structures. The bigger the scattering particle is, the more forward-oriented is the scattered light intensity.[44] This observation is consistent with a decrease in the illuminated area as the number of scatterers is reduced, and their size increases. The latter approach would be a simplification because the *rouleaux* are complex branched 3D structures and not spherical particles.

On the one hand, the RBCs suspended in plasma showed less susceptibility to the effects of dex500. However, differentiated behaviors were observed as the erythrocyte aggregation occurs. The CIs approached the -1 to -2 value range as the sample decreases its activity with time and reaches saturation in structure formation. On the other hand, the CIs for the RBCs suspended in PBS with dex500 assumed a wide range of values (-2 to -8). It is important to note that erythrocyte aggregation is analyzed in several degrees leading to different structure size distributions since scenarios vary from isolated cells to the formation of clusters. As the reference time is higher, the CIs tend to have a stabilized value for each sample. We can point out that the final values of CIs are different for each concentration of dex500, being an indicator of the degree of RBC aggregation at the end.

In the case of RBC in plasma, the IM values are within the 100 to 125 range for the dex500 concentration. Further, it remained constant within the uncertainty, which would support the hypothesis of its dependency on hematocrit, as occurs for subjective FSC-BSL.[33] An activity decrease is observed in the sample of RBCs suspended in PBS with dex500 at 1.2 g/dL. This low activity can be related to a rapid formation of structures, less isolated cells, and the early appearance of sedimentation. This parameter represents the sample dynamics for different RBC aggregation states. Therefore, a "reference range" could be established for comparing different blood samples.

Variations in the BSL grain size were recorded for plasma with dex500 and PBS with dex500 suspension media. The index S_g presented a more marked time dependence for RBCs in PBS with dex500. The growth of S_g is similar between the RBCs in plasma media, and the polynomial fit coefficients follow the same trend as in the case of RBCs in PBS with dex500. *In vitro* erythrocyte aggregation ranging from isolated RBCs to the formation of clusters results in traces of S_g with a faster-increasing behavior as the dex500 concentration is higher in the sample. This behavior is observed in the variation of the polynomial fit coefficients and the grain size change.

The gap in the S_g initial value is reproduced in the PBS-dex500 media but in a more evenly distributed fashion than the corresponding to plasma-dex500 media. These initial differences are attributed to the presence of structures that have not been disaggregated before the recording, and it is expected that they will be more abundant as the dex500 concentration increases in the suspension medium. The formation of linear structures that require higher shear stresses to disaggregate occurs for dex500 concentrations close to- and greater than 1 g/dL. In this sense, more RBC aggregate morphologies can reach the condition of "cluster."[7]

The S_g fitting was carried out, and characteristic coefficients of the erythrocyte aggregation were obtained to help the identification of anomalies (for example, in vascular pathologies). Particularly, the polynomial fit coefficients give information about the type of grain size growth as they characterize the shape of the grain size versus time. The experimental data were fitted using the best polynomial fit to characterize three stages: initial growth, slight plateau, and final growth. The polynomial coefficients are related to each experimental sample and describe the time evolution of S_g. In particular, the linear coefficient B1 is the most sensitive to the dex500 concentration. The B3 coefficient shows a steep growth of the grain size versus time after a slight plateau in the S_g evolution. At that stage, RBC sedimentation occurs as commonly expected and

described by Fabry.[45] The presence of dextran in the suspension medium would induce early sedimentation of erythrocyte aggregates Consequently, the B3 coefficient may be associated with the sedimentation phenomenon.[46] The BSL grain size monitoring contains information on both the dynamics and the morphology of the scattering element. The development of this technique is aimed to further contribute to non-invasive diagnostic technologies related to the study of blood and the interaction of its components. It would be possible to describe particular states of erythrocyte aggregation using the S_g parameter and differentiate pathological conditions of the blood. In this way, by standardizing the measurement device, controlling variables, such as the distance of the sample to the image plane, and compacting the experimental arrangement, it would be possible to develop a portable device for the study of erythrocyte aggregation based on BSL.

Acknowledgments

The authors would like to thank Dr. Analía Alet of the FCByF (UNR) for her help and expertise in the sample preparation. This work was financially supported by CONICET (Grant No. PIP 11220150100607) and UNR (Grant Nos. PI BIO400 and 80020190300107UR), Argentina. Martín A. Toderi thanks CONICET for its fellowship during his doctoral thesis.

References

1. T. J. McMahon, "Red blood cell deformability, vasoactive mediators, and adhesion," *Front. Physiol.* **10**, 1417 (2019).
2. S. Chien and K. M. Jan, "Ultrastructural basis of the mechanism of rouleaux formation," *Microvasc. Res.* **5**(2), 155–166 (1973).
3. S. Chien and L. A. Sung, "Physicochemical basis and clinical implications of red cell aggregation," *Clin. Hemorheol.* **7**(1), 71–91 (1987).
4. F. A. Carvalho et al., "Atomic force microscopy-based molecular recognition of a fibrinogen receptor on human erythrocytes," *ACS Nano* **4**(8), 4609–4620 (2010).
5. C. E. Ioan, T. Aberle, and W. Burchard, "Light scattering and viscosity behavior of dextran in semidilute solution," *Macromolecules* **34**(2), 326–336 (2001).
6. M. Koralewski et al., "Optical and magnetooptical properties of clinical dextrans," *Acta Physica Pol. Ser. A* **112**(5), 1119 (2007).
7. B. Neu, R. Wenby, and H. J. Meiselman, "Effects of dextran molecular weight on red blood cell aggregation," *Biophys. J.* **95**(6), 3059–3065 (2008).
8. D. E. Brooks, "Mechanism of red cell aggregation," in *Blood Cells, Rheology, and Aging*, pp. 158–162, Springer, Berlin, Heidelberg (1988).
9. C. Wagner, P. Steffen, and S. Svetina, "Aggregation of red blood cells: from rouleaux to clot formation," *C. R. Phys.* **14**(6), 459–469 (2013).
10. B. Neu and H. J. Meiselman, "Depletion-mediated red blood cell aggregation in polymer solutions," *Biophys. J.* **83**(5), 2482–2490 (2002).
11. B. Neu and H. J. Meiselman, *The Role of Macromolecules in Stabilization and De-Stabilization of Biofluids*, pp. 393–414, Springer, Berlin, Heidelberg (2008).
12. R. Fantoni, A. Giacometti, and A. Santos, "Bridging and depletion mechanisms in colloid-colloid effective interactions: a reentrant phase diagram," *J. Chem. Phys.* **142**(22), 224905 (2015).
13. S. K. Doddi and P. Bagchi, "Three-dimensional computational modeling of multiple deformable cells flowing in microvessels," *Phys. Rev. E* **79**, 046318 (2009).
14. B. Riquelme, H. Castellini, and B. Albea, "Linear and non-linear viscoelasticity of red blood cells using a new optical erythrocyte rheometer," in *Latin Am. Opt. and Photonics Conf.*, Optical Society of America, p. Th4A.41 (2018).
15. T. Ye et al., "Hybrid smoothed dissipative particle dynamics and immersed boundary method for simulation of red blood cells in flows," *Phys. Rev. E* **95**, 063314 (2017).
16. M. Delannoy et al., "Arterial hypertension modeled by in vitro treatment of red blood cells with trypsin," *Ser. Biomech.* **27**, 87–92 (2012).

17. M. Delannoy et al., "Influence of hypertension and diabetes mellitus on erythrocyte aggregation using image digital analysis," *Ser. Biomech.* **29**(1), 5–10 (2015).
18. E. Kaliviotis et al., "Quantifying local characteristics of velocity, aggregation and hematocrit of human erythrocytes in a microchannel flow," *Clin. Hemorheol. Microcirc.* **63**(2), 123–148 (2016).
19. D. Pinho et al., "In vitro particulate analogue fluids for experimental studies of rheological and hemorheological behavior of glucose-rich RBC suspensions," *Biomicrofluidics* **11**(5), 054105 (2017).
20. H. Lim et al., "Measurement of blood coagulation with considering RBC aggregation through a microchip-based light transmission aggregometer," *Clin. Hemorheol. Microcirc.* **47**(3), 211–218 (2011).
21. B. D. Riquelme et al., "Analysis of the 3D structure of agglutinated erythrocyte," *Prog. Biomed. Opt. Imaging* **4**(28), 190–198 (2003).
22. B. D. Riquelme et al., "Analysis of the 3D structure of agglutinated erythrocyte using CellScan and confocal microscopy: characterization by FLIM-FRET," *Proc. SPIE* **5139**, 190–198 (2003).
23. L. Plá et al., "Cold-agglutinin hemolytic diseases, a rheo-optical study," *Clin. Hemorheol. Microcirc.* **38**(2), 83–91 (2008).
24. S. Shin et al., "Shear-dependent aggregation characteristics of red blood cells in a pressure driven microfluidic channel," *Clin. Hemorheol. Microcirc.* **34**(1–2), 353–362 (2006).
25. D. E. McMillan, "Hemorheological studies in the diabetes control & complications trial," *Clin. Hemorheol. Microcirc.* **13**(2), 147–154 (1993).
26. O. K. Baskurt and H. J. Meiselman, "Erythrocyte aggregation: basic aspects and clinical importance," *Clin. Hemorheol. Microcirc.* **53**(1–2), 23–37 (2013).
27. M. A. Toderi, H. V. Castellini, and B. D. Riquelme, "Descriptive parameters of the erythrocyte aggregation phenomenon using a laser transmission optical chip," *J. Biomed. Opt.* **22**(1), 017003 (2017).
28. R. Jones and K. Wykes, *Holographic and Speckle Interferometry*, Cambridge Studies in Modern Optics, 2nd ed., Cambridge University Press (1989).
29. S. M. White, S. C. George, and B. Choi, "Automated computation of functional vascular density using laser speckle imaging in a rodent window chamber model," *Microvasc. Res.* **82**(1), 92–95 (2011).
30. M. Z. Ansari and A. K. Nirala, "Biospeckle assessment of torn plant leaf tissue and automated computation of leaf vein density (LVD)," *Eur. Phys. J. Appl. Phys.* **70**(2), 21201 (2015).
31. R. A. Braga et al., "Dynamic laser speckle analyzed considering inhomogeneities in the biological sample," *J. Biomed. Opt.* **22**(4), 045010 (2017).
32. R. R. Cardoso et al., "Frequency signature of water activity by biospeckle laser," *Opt. Commun.* **284**(8), 2131–2136 (2011).
33. M. A. Toderi, B. D. Riquelme, and G. E. Galizzi, "An experimental approach to study the red blood cell dynamics in a capillary tube by biospeckle laser," *Opt. Lasers Eng.* **127**, 105943 (2020).
34. O. K. Baskurt et al., "New guidelines for hemorheological laboratory techniques," *Clin. Hemorheol. Microcirc.* **42**(2), 75–97 (2009).
35. M. Vetterli and C. Herley, "Wavelets and filter banks: theory and design," *IEEE Trans. Signal Process.* **40**(9), 2207–2232 (1992).
36. S. K. Agrawal and O. P. Sahu, "Two-channel quadrature mirror filter bank: an overview," *ISRN Signal Process.* **2013**, 815619 (2013).
37. R. Cardoso and R. Braga, "Enhancement of the robustness on dynamic speckle laser numerical analysis," *Opt. Lasers Eng.* **63**, 19–24 (2014).
38. R. Arizaga, M. Trivi, and H. Rabal, "Speckle time evolution characterization by the co-occurrence matrix analysis," *Opt. Laser Technol.* **31**(2), 163–169 (1999).
39. A. Oulamara, G. Tribillon, and J. Duvernoy, "Biological activity measurement on botanical specimen surfaces using a temporal decorrelation effect of laser speckle," *J. Mod. Opt.* **36**(2), 165–179 (1989).

40. R. Braga et al., "Biological feature isolation by wavelets in biospeckle laser images," *Comput. Electron. Agric.* **58**(2), 123–132 (2007).
41. R. A. Braga et al., "Live biospeckle laser imaging of root tissues," *Eur. Biophys. J.* **38**, 679–686 (2009).
42. Y. Piederrière et al., "Backscattered speckle size as a function of polarization: influence of particle-size and -concentration," *Opt. Express* **13**(13), 5030–5039 (2005).
43. Y. Piederriere et al., "Particle aggregation monitoring by speckle size measurement; application to blood platelets aggregation," *Opt. Express* **12**(19), 4596–4601 (2004).
44. H. Rabal and R. Braga, *Dynamic Laser Speckle and Applications*, CRC Press, Boca Raton, FL (2009).
45. T. L. Fabry, "Mechanism of erythrocyte aggregation and sedimentation," *Blood* **70**(5), 1572–1576 (1987).
46. E. Kaliviotis and M. Yianneskis, "Blood viscosity modelling: influence of aggregate network dynamics under transient conditions," *Biorheology* **48**(2), 127–147 (2011).

Martín A. Toderi received his PhD in physics from National University of Rosario in 2020. He is a postdoctoral scholar in the Physics and Astronomy Department, University of California Los Angeles. His current research interests are neurophotonics, biospeckle, and hair cells mechanics. He is a member of SPIE.

Bibiana D. Riquelme received his doctorate degree in physics from National University of Rosario in 1997. Currently, she is a principal researcher at UNR Research Council and a physics professor at Faculty of Biochemical and Pharmaceutical Sciences, National University of Rosario. She is the director of the Biomedical Physics Group at Rosario Institute of Physics (CONICET-UNR). She has extensive experience in biophotonics and biomechanics, particularly in hemorheology.

Gustavo E. Galizzi received his PhD in engineering from National University of Rosario in 2003. He is an adjunct researcher from CONICET at the Institute of Physics Rosario. His research is focused on optical metrology conducted at Optics and Photonics group.

Queries

1. Please confirm the corresponding author e-mail address.
2. Please check the sentence "In particular, the . . ." for correctness.
3. Please provide the expansion of EDTA.
4. Please check whether the edits made in the sentence "All other microscopic . . ." are correct.
5. The DOIs for references [16, 17, 21, 23, and 24] could not be located in the CrossRef database. While these references may be correct, we ask that you check them for accuracy so we can provide as many DOI links to the referenced articles as possible.
6. Please provide editor name for Reference 8.

Funding Information

The authors have identified the following funders and award numbers, either on the submission form at the time of submission or in the Acknowledgments of the manuscript. Please check this list of funding agencies and make any necessary corrections using the full and official name of the funding organization. You may also wish to edit the Acknowledgments, if needed. This information may be used to help SPIE comply with funding reporting mandates.

- CONICET; Award no. PIP 11220150100607
- UNR; Award no(s). PI BIO400, 80020190300107UR